THIRD ORDER NONOSCILLATORY CENTRAL SCHEME
FOR HYPERBOLIC CONSERVATION LAWS

XU-DONG LIU[†]   AND   EITAN TADMOR[‡§]

Abstract. A third-order accurate Godunov-type scheme for the approximate solution of hyperbolic systems of conservation laws is presented. Its two main ingredients include: #1. A non-oscillatory piecewise-quadratic reconstruction of pointvalues from their given cell averages; and #2. A central differencing based on *staggered* evolution of the reconstructed cell averages. This results in a third-order central scheme, an extension along the lines of the second-order central scheme of Nessyahu and Tadmor [NT]. The scalar scheme is non-oscillatory (and hence – convergent), in the sense that it does not increase the *number* of initial extrema (–as does the exact entropy solution operator).

Extension to systems is carried out by *componentwise* application of the scalar framework. In particular, we have the advantage that, unlike upwind schemes, no (approximate) Riemann solvers, field-by-field characteristic decompositions, etc., are required. Numerical experiments confirm the high-resolution content of the proposed scheme. Thus, a considerable amount of simplicity and robustness is gained while retaining the expected third-order resolution.

Contents. 1 Introduction   **1**

[†] Courant Institute of Mathematical Sciences, 251 Mercer Street, New York, NY 10012; Email: xliu@cims.nyu.edu

[‡] School of Mathematical Sciences, Tel-Aviv University, Tel-Aviv 69978 Israel

[§] Department of Mathematics, UCLA, Los-Angeles CA 90095; Email: tadmor@math.ucla.edu

1. Introduction. In this paper we present a third-order, non-oscillatory central difference scheme for the approximate solution of nonlinear systems of hyperbolic conservation laws. The scheme can be viewed as natural next step in the sequel to the first-order Lax-Friedrichs(LxF) scheme, and the second-order central scheme of Nessyahu and Tadmor, [NT]. Our third-order scheme enjoys a major advantage of the central schemes over the upwind ones, in that no Riemann solvers are involved. The use of third-order piecewise-quadratic approximation compensates for the excessive viscosity typical to the first-order LxF piecewise-constant solution, and it offers an improved resolution beyond the second-order piecewise-linear approximation used in [NT]. The result is a simple, robust, Riemann-solver-free central difference scheme with third-order resolution.

In §2, we provide a self-contained discussion on Godunov-type schemes. Such schemes are based on piecewise-polynomial *reconstruction* — reconstruction of point-values from cell averages, followed by an *evolution* step — the evolution of approximate fluxes. Our point of view is that the distinction between upwind and central Godunov-type schemes, lies in the way they *realize* the evolution of these piecewise-polynomials: Upwind schemes sample the reconstructed values at the *mid-cells*; central schemes are based on *staggered* sampling at the interfacing *breakpoints*.

In §3, we recall the non-oscillatory third-order accurate reconstruction due to Liu & Osher [LO], and combine it with central differencing, based on *staggered* sampling along the lines of [NT]. Thus, at each time-level, we reconstruct from the given cell-averages, a non-oscillatory piecewise-quadratic approximation of third-order accuracy. We then follow the evolving solution to the next time level, and end up by projecting back the staggered cell-averages of the solution.

In §4 we take a closer look at the non-oscillatory character of our scalar third-order scheme, proving it is non-oscillatory in the sense of satisfying the Number of Extrema Diminishing (NED) property; this, together with an L^∞-bound imply the total-variation boundedness and hence the convergence of the third-order approximate solution.

Finally, in §5 we present numerical experiments with our third-order, non-oscillatory central difference scheme. Both the quantitative and qualitative results for a representative sample of compressible flow problems governed by Euler equations, are found to be in complete agreement with the high resolution expected by the scalar analysis. Taking into account the ease of implementation, robustness and time performance, these results compare favorably with the results obtained by the corresponding upwind-based schemes. Similar results regarding the advantages of *central* over *upwind* schemes in robustness, efficiency and simplicity, were concluded by e.g., Sanders, [Sa1],[Sa2], and Huynh, [Hu], and were further amplified by our numerical experiments in the forthcoming [JT], [TW].

We conclude this Introduction with a brief overview of previous work on non-oscillatory schemes of third-order accuracy. The first pioneering work in this category is due to Colella and Woodward, [CW]. Their PPM method, as well as the third-order versions of the ENO scheme, [HEOC], [Sh], integrate a co-monotonicity constrained piecewise-parabolic reconstruction into the framework of *upwind* Godunov-type scheme. Sanders [Sa1], and Sanders and Weiser [SW], introduced a third-order *central*

scheme which satisfies the Total-Variation Diminishing (TVD) property; to circumvent the second-order limitation of TVD schemes, [OT], Sanders advances both — mid-cell averages and interface pointvalues. The latter, however, were evolved by ray tracing which require the complexity of characteristic information. Finally, Huynh, [Hu], simplifies Sanders' approach, using his own co-monotone piecewise-parabolic reconstruction augmented with pointwise evolution along the lines of [NT].

2. Godunov-type schemes. We want to solve the hyperbolic system of conservation laws

$$(2.1) \qquad u_t + f(u)_x = 0$$

by Godunov-type schemes. To this end we proceed in two steps. First, we introduce a small spatial scale, Δx, and we consider the corresponding (Steklov) sliding average of $u(\cdot, t)$,

$$\bar{u}(x, t) := \frac{1}{|I_x|} \int_{I_x} u(\xi, t) d\xi, \qquad I_x = \left\{ \xi \mid |\xi - x| \leq \frac{\Delta x}{2} \right\}.$$

The sliding average of (2.1) then yields

$$(2.2) \qquad \bar{u}_t(x, t) + \frac{1}{\Delta x} \left[f(u(x + \frac{\Delta x}{2}, t)) - f(u(x - \frac{\Delta x}{2}, t)) \right] = 0.$$

Next, we introduce a small time-step, Δt, and integrate over the slab $t \leq \tau \leq t + \Delta t$,

$$(2.3) \quad \bar{u}(x, t + \Delta t) = \bar{u}(x, t)$$
$$- \frac{1}{\Delta x} \left[\int_{\tau=t}^{t+\Delta t} f(u(x + \frac{\Delta x}{2}, \tau)) d\tau - \int_{\tau=t}^{t+\Delta t} f(u(x - \frac{\Delta x}{2}, \tau)) d\tau \right].$$

We end up with an equivalent reformulation of the conservation law (2.1): it expresses the precise relation between the sliding averages, $\bar{u}(\cdot, t)$, and their underlying pointvalues, $u(\cdot, t)$. We shall use this reformulation, (2.3), as the starting point for the construction of Godunov-type schemes.

We construct an approximate solution, $w(\cdot, t^n)$, at the discrete time-levels, $t^n = n\Delta t$. Here, $w(x, t^n)$ is a piecewise polynomial written in the form

$$w(x, t^n) = \sum p_j(x) \chi_j(x), \quad \chi_j(x) := 1_{I_j},$$

where $p_j(x)$ are algebraic polynomials supported at the discrete cells, $I_j = I_{x_j}$, centered around the midpoints, $x_j := j\Delta x$. An *exact* evolution of $w(\cdot, t^n)$ based on (2.3), reads

$$(2.4) \quad \bar{w}(x, t^{n+1}) = \bar{w}(x, t^n)$$
$$- \frac{1}{\Delta x} \left[\int_{t^n}^{t^{n+1}} f(w(x + \frac{\Delta x}{2}, \tau)) d\tau - \int_{t^n}^{t^{n+1}} f(w(x - \frac{\Delta x}{2}, \tau)) d\tau \right].$$

To construct a Godunov-type scheme, we *realize* (2.4) — or at least an accurate approximation of it, at discrete gridpoints. Here, we distinguish between the main methods, according to their way of *sampling* (2.4): these two main sampling methods correspond to upwind schemes and central schemes.

2.1. Upwind schemes. Let $\bar{w}_\nu^n$ abbreviates the cell averages, $\bar{w}_\nu^n := \frac{1}{\Delta x} \int_{I_\nu} w(\xi, t^n) d\xi$. By sampling (2.4) at the *mid-cells*, $x = x_\nu$, we obtain an evolution scheme for these averages, which reads

$$(2.5) \qquad \bar{w}_\nu^{n+1} = \bar{w}_\nu^n - \frac{1}{\Delta x} \left[\int_{\tau=t^n}^{t^{n+1}} f(w(x_{\nu+\frac{1}{2}}, \tau)) d\tau - \int_{\tau=t^n}^{t^{n+1}} f(w(x_{\nu-\frac{1}{2}}, \tau)) d\tau \right].$$

Here, it remains to recover the *pointvalues*, $\{w(x_{\nu+\frac{1}{2}}, \tau)\}_\nu$, $t^n \leq \tau \leq t^{n+1}$, in terms of their known cell averages, $\{\bar{w}_\nu^n\}_\nu$, and to this end we proceed in two steps:

- First, the *reconstruction* – we recover the pointwise values of $w(\cdot, \tau)$ at $\tau = t^n$, by a reconstruction of a piecewise polynomial approximation

$$(2.6) \qquad w(x, t^n) = \sum_j p_j(x) \chi_j(x), \quad \bar{p}_\nu(x_\nu) = \bar{w}_\nu^n.$$

- Second, the *evolution* — $w(x_{\nu+\frac{1}{2}}, \tau \geq t^n)$ are determined as the solutions of the generalized Riemann problems

$$(2.7) \qquad w_t + f(w)_x = 0, \quad t \geq t^n; \quad w(x, t^n) = \begin{cases} p_\nu(x) & x < x_{\nu+\frac{1}{2}}, \\ p_{\nu+1}(x) & x > x_{\nu+\frac{1}{2}}. \end{cases}$$

The solution of (2.7) is composed of a family of nonlinear waves – left-going and right-going waves. An exact Riemann solver, or at least an approximate one is used to distribute these nonlinear waves between the two neighboring cells, I_ν and $I_{\nu+1}$. It is this distribution of waves according to their direction which is responsible for *upwind differencing*, consult Figure 2.1. We briefly recall few canonical examples for this category of upwind Godunov-type schemes.
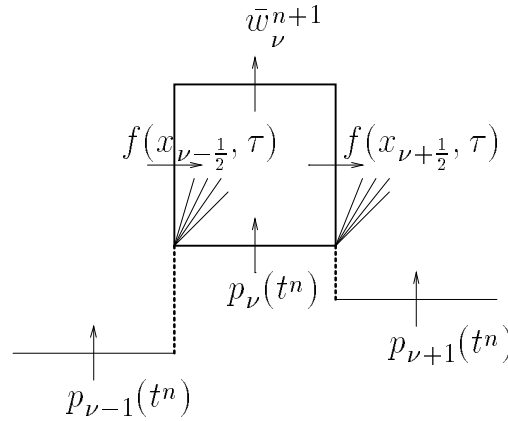

Fig. 2.1: Upwind differencing by Godunov-type scheme.

The original Godunov scheme is based on piecewise-constant reconstruction, $w(x, t^n) = \Sigma \bar{w}_j^n \chi_j$, followed by an exact Riemann solver. This results in a first-order accurate upwind method [Go], which is the forerunner for all other Godunov-type schemes. A second-order extension was introduced by van Leer [Le]: his MUSCL scheme reconstructs a piecewise linear approximation, $w(x, t^n) = \Sigma p_j(x)\chi_j(x)$, with linear pieces of the form $p_j(x) = \bar{w}_j^n + w_j'\left(\frac{x-x_j}{\Delta x}\right)$ so that $\bar{p}_j(x_j) = \bar{w}_j^n$. Here the w_j'-s are possibly limited slopes which are reconstructed from the known cell-averages, $w_j' = \{(w_j^n)'\} = \{w'(\bar{w}_k^n)_{k=j-1}^{j+1}\}$. (Throughout the paper we use primes, $w_j', w_j'', \ldots$, to denote *discrete* derivatives, which approximate the corresponding differential ones). A whole library of limiters is available in this context, so that the co-monotonicity of $w(x, t^n)$ with $\Sigma \bar{w}_j \chi_j$ is guaranteed, e.g., [Sw]. The Piecewise-Parabolic Method (PPM) of Woodward-Colella [CW] and respectively, ENO schemes of Harten et.al. [HEOC], offer, respectively, third- and higher-order Godunov-type upwind schemes. Fianlly, we should not give the impression that limiters are used exclusively in conjunction with Godunov-type schemes. The *positive schemes* of Liu and Lax, [LL], offer simple and fast upwind schemes for multidimensional systems, based on an alternative positivity principle.

2.2. Central schemes. As before, we seek a piecewise-polynomial, $w(x, t^n) = \Sigma p_j(x)\chi_j(x)$, which serves as an approximate solution to the *exact* evolution of sliding averages in (2.4),

$$\bar{w}(x, t^{n+1}) = \bar{w}(x, t^n) - \frac{1}{\Delta x}\left[\int_{t^n}^{t^{n+1}} f(w(x + \frac{\Delta x}{2}, \tau))d\tau - \int_{t^n}^{t^{n+1}} f(w(x - \frac{\Delta x}{2}, \tau))d\tau\right].$$

(2.8)

Note that the polynomial pieces of $w(x, t^n)$ are supported in the cells, $I_\nu = \left\{\xi \mid |\xi - x_\nu| \le \frac{\Delta x}{2}\right\}$, with interfacing breakpoints at the half-integers gridpoints, $x_{\nu+\frac{1}{2}} = \left(\nu + \frac{1}{2}\right)\Delta x$.

We recall that upwind schemes (2.5) were based on sampling (2.4) in the *midcells*, $x = x_\nu$. In contrast, central schemes are based on sampling (2.8) at the *interfacing breakpoints*, $x = x_{\nu+\frac{1}{2}}$, which yields

$$(2.9) \qquad \bar{w}_{\nu+\frac{1}{2}}^{n+1} = \bar{w}_{\nu+\frac{1}{2}}^n - \frac{1}{\Delta x}\left[\int_{\tau=t^n}^{t^{n+1}} f(w(x_{\nu+1}, \tau))d\tau - \int_{\tau=t^n}^{t^{n+1}} f(w(x_\nu, \tau))d\tau\right].$$

We want to utilize (2.9) in terms of the known cell averages at time level $\tau = t^n$, $\{\bar{w}_\nu^n\}_\nu$. The remaining task is therefore to recover the *pointvalues* $\{w(\cdot, \tau)\mid t^n \le \tau \le t^{n+1}\}$, and in particular, the *staggered averages*, $\{\bar{w}_{\nu+\frac{1}{2}}^n\}$. As before, this task is accomplished in two main steps:

- First, we use the given cell averages $\{\bar{w}_\nu^n\}_\nu$, to *reconstruct* the pointvalues of $w(\cdot, \tau = t^n)$ as piecewise polynomial approximation

$$(2.10) \qquad w(x, t^n) = \sum_j p_j(x)\chi_j(x), \quad \bar{p}_\nu(x_\nu) = \bar{w}_\nu^n.$$

In particular, the staggered averages on the right of (2.9) are given by

$$(2.11) \qquad \bar{w}_{\nu+\frac{1}{2}}^n = \frac{1}{\Delta x}\left[\int_{x_\nu}^{x_{\nu+\frac{1}{2}}} p_\nu(x)dx + \int_{x_{\nu+\frac{1}{2}}}^{x_{\nu+1}} p_{\nu+1}(x)dx\right].$$

The resulting central scheme (2.9) then reads

$$(2.12) \quad \bar{w}^{n+1}_{\nu+\frac{1}{2}} \quad = \quad \frac{1}{\Delta x} \left[\int_{x_\nu}^{x_{\nu+\frac{1}{2}}} p_\nu(x)dx + \int_{x_{\nu+\frac{1}{2}}}^{x_{\nu+1}} p_{\nu+1}(x)dx \right] +$$

$$- \quad \frac{1}{\Delta x} \left[\int_{\tau=t^n}^{t^{n+1}} f(w(x_{\nu+1},\tau))d\tau - \int_{\tau=t^n}^{t^{n+1}} f(w(x_\nu,\tau))d\tau \right].$$

- Second, we follow the *evolution* of the pointvalues along the mid-cells, $x = x_\nu$, $\{w(x_\nu, \tau \geq t^n)\}_\nu$, which are governed by

$$(2.13) \qquad w_t + f(w)_x = 0, \quad \tau \geq t^n; \quad w(x,t^n) = p_\nu(x) \quad x \in I_\nu.$$

Let $\{a_k(u)\}_k$ denote the eigenvalues of the Jacobian $A(u) := \frac{\partial f}{\partial u}$. By hyperbolicity, information regarding the interfacing discontinuities at $(x_{\nu \pm \frac{1}{2}}, t^n)$ propagates no faster than $\max_k |a_k(u)|$. Hence, the mid-cells values governed by (2.13), $\{w(x_\nu, \tau \geq t^n)\}_\nu$, remain free of discontinuities, at least for sufficiently small time step dictated by the CFL condition $\Delta t \leq \frac{1}{2}\Delta x \cdot \max_k |a_k(u)|$. Consequently, since the numerical fluxes on the right of (2.12), $\int_{\tau=t^n}^{t^{n+1}} f(w(x_\nu,\tau))d\tau$, involve only smooth integrands, they can be computed within any degree of desired accuracy by an appropriate quadrature rule.

It is the *staggered* averaging over the fan of left-going and right-going waves centered at the half-integered interfaces, $(x_{\nu+\frac{1}{2}}, t^n)$, which characterizes the *central* differencing, consult Figure 2.2. A main feature of these central schemes – in contrast to upwind ones, is the computation of *smooth* numerical fluxes along the mid-cells, $(x = x_\nu, \tau \geq t^n)$, which avoids the costly (approximate) Riemann solvers. A couple of examples of central Godunov-type schemes is in order.
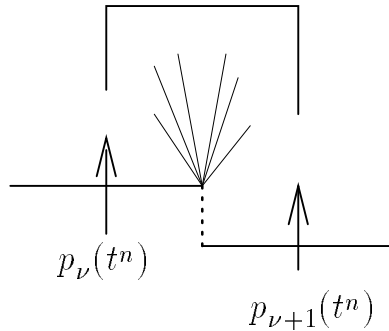

Fig. 2.2: Central differencing by Godunov-type scheme.

The first-order Lax-Friedrichs (LxF) approximation is the forerunner for such central schemes — it is based on piecewise constant reconstruction, $w(x, t^n) = \Sigma p_j(x)\chi_j(x)$ with

$p_j(x) = \bar{w}_j^n$. The resulting central scheme, (2.12), then reads (with the usual fixed mesh ratio $\lambda := \frac{\Delta t}{\Delta x}$)

$$(2.14) \qquad \bar{w}_{\nu+\frac{1}{2}}^{n+1} = \frac{1}{2}(\bar{w}_\nu + \bar{w}_{\nu+1}) - \lambda\Big[f(\bar{w}_{\nu+1}) - f(\bar{w}_\nu)\Big].$$

Nessyahu and Tadmor introduced in [NT] a second-order extension along these lines. Using the piecewise-linear MUSCL reconstruction,

$$w(x, t^n) = \sum p_j(x)\chi_j(x), \quad \text{with } p_j(x) = \bar{w}_j^n + w_j'\left(\frac{x - x_j}{\Delta x}\right),$$

leads to a straightforward evaluation of staggered averages

$$(2.15) \qquad \bar{w}_{\nu+\frac{1}{2}}^n := \frac{1}{\Delta x}\int_{x_j}^{x_{n+1}} w(x, t^n)dx = \frac{1}{2}(\bar{w}_\nu^n + \bar{w}_{\nu+1}^n) + \frac{1}{8}(w_\nu' - w_{\nu+1}').$$

The numerical flux is approximated by the second-order midpoint quadrature rule

$$\int_{\tau=t^n}^{t^{n+1}} f(w(x_\nu, \tau))d\tau \sim \Delta t \cdot f(w(x_\nu, t^{n+\frac{1}{2}})).$$

Here, the pointwise values at the half-time steps are evaluated by Taylor expansion (– recall the smoothness of (2.13) along the cell interfaces, $(x_\nu, \tau \geq t^n)$),

$$
\begin{aligned}
w(x_\nu, t^{n+\frac{1}{2}}) &\sim w(x_\nu, t) + \frac{\Delta t}{2}w_t(x_\nu, t^n) \\
&= \bar{w}_\nu^n - \frac{\Delta t}{2}A(\bar{w}_\nu^n)(p_\nu(x_\nu, t^n))_x = \bar{w}_\nu^n - \frac{\lambda}{2}A_\nu^n w_\nu'.
\end{aligned}
$$

In summary, we end up with the central scheme, [NT], which consists of a first-order *predictor step*,

$$(2.16) \qquad w_\nu^{n+\frac{1}{2}} = \bar{w}_\nu^n - \frac{\lambda}{2}A_\nu^n w_\nu', \qquad A_\nu^n := A(\bar{w}_\nu^n),$$

followed by the second-order *corrector step*, (2.12),

$$(2.17) \qquad \bar{w}_{\nu+\frac{1}{2}}^{n+1} = \frac{1}{2}(\bar{w}_\nu^n + \bar{w}_{\nu+1}^n) + \frac{1}{8}(w_\nu' - w_{\nu+1}') - \lambda\left[f(w_{\nu+1}^{n+\frac{1}{2}}) - f(w_\nu^{n+\frac{1}{2}})\right].$$

The *scalar* non-oscillatory properties of (2.16)-(2.17) were proved in [NT],[NTT], including TVD, cell entropy inequality, L_{loc}^1 – error estimates.... . Moreover, the numerical experiments, reported in [Ne], [NT], [ASV], [TW], with one- and multi-dimensional *systems* of conservation laws, show that such second-order central schemes enjoy the same high-resolution as the corresponding second-order upwind schemes do. Thus, the excessive smearing typical to the first-order LxF central scheme is compensated here by the second-order accurate MUSCL reconstruction.

At the same time, the central scheme (2.16)-(2.17) has the advantage over the corresponding upwind schemes, in that no (approximate) Riemann solvers, as in (2.7), are

required. Hence, these Riemann-free central schemes provide an efficient high-resolution alternative in the one-dimensional case, and a particularly advantageous framework for multidimensional computations, e.g., [AV],[ASV], [JT]. Also, *staggered* central differencing, along the lines of the Riemann-free Nessyahu-Tadmor scheme (2.16)-(2.17), admits simple efficient extensions in the presence of general source terms, [Er], and in particular, stiff source terms, [BS]. Indeed, it is a key ingredient behind the relaxation schemes studied in [JX],...

It should be noted, however, that the component-wise version of these central schemes might result in deterioration of resolution at the computed extrema. Of course, this – so called extrema clipping, is typical to high-resolution upwind schemes as well; but it is more pronounced with our central schemes due to the built-in extrema-switching to the dissipative LxF scheme. Indeed, once an extrema cell, I_ν, is detected (by the limiter), it sets a zero slope, $w'_\nu = 0$, in which case the second-order scheme (2.16)-(2.17) is reduced back to the first-order LxF, (2.14).

With this in mind, we now turn to discuss a *third-order* accurate Godunov-type central scheme along the above lines. It offers an improved resolution over the second-order central scheme (2.16)-(2.17), and in particular, this additional accuracy compensates for the lost resolution at the clipped extrema.

3. Third-order central Godunov-type scheme. In this section we introduce our new third-order, non-oscillatory central Godunov-type scheme. Following the framework outlined in §2, the construction of such scheme consists of two main ingredients:

(i) A third-order, piecewise-quadratic polynomial reconstruction which enjoys desirable non-oscillatory properties;

(ii) An appropriate quadrature rule to approximate the numerical fluxes along cells' interfaces.

We first address the *scalar* problem. And again, it should be reminded that since our central scheme avoids (approximate) Riemann solvers, its extension to *systems* may proceed by a straightforward *component-wise* application of the scalar recipe — no characteristic decompositions are required.

3.1. Third-order non-oscillatory reconstruction. We shall use the third-order non-oscillatory reconstruction of Liu & Osher [LO]. Here is a reader's digest for this reconstruction.

We start by seeking quadratic polynomials, $q_j(x) = a_j + b_j \left(\frac{x-x_j}{\Delta x}\right) + c_j \left(\frac{x-x_j}{\Delta x}\right)^2$, such that the piecewise parabolic reconstruction, $w(x, t^n) = \Sigma q_j(x)\chi_j(x)$, satisfies the two properties of:

$\mathcal{P}_1$ *Conservation.* Conserving the given cell-averages, $\{\bar{w}_j^n\}_j$

$$(3.1) \qquad\qquad\qquad \bar{w}(x, t^n)_{|x=x_j} = \bar{w}_j^n$$

$\mathcal{P}_2$ *Accuracy.* Third-order accuracy

$$(3.2) \qquad\qquad\qquad w(x, t^n) = u(x, t^n) + \mathcal{O}((\Delta x)^3).$$

To satisfy $\mathcal{P}_1$ and $\mathcal{P}_2$, one constructs a quadratic polynomial, $q_j(x)$, whose sliding averages interpolate $\bar{w}_j$ (– that is, property $\mathcal{P}_1$), *and*, in addition, it interpolates the

two neighboring cell averages, $\bar{w}^n_{j\pm1}$. The three constrains then determine the unique parabola[1]

$$(3.3) \quad q_j(x) = \left(\bar{w}^n_j - \frac{1}{24}\Delta_+\Delta_-\bar{w}^n_j\right) + \Delta_0\bar{w}^n_j\left(\frac{x - x_j}{\Delta x}\right) + \frac{1}{2}\Delta_+\Delta_-\bar{w}^n_j \cdot \left(\frac{x - x_j}{\Delta x}\right)^2,$$

which satisfies both (3.1) and (3.2). Moreover, since

$$q'_j(x_{j-\frac{1}{2}})q'_j(x_{j+\frac{1}{2}}) = \Delta_-\bar{w}_j \cdot \Delta_+\bar{w}_j/(\Delta x)^2,$$

it follows that the quadratic reconstruction in (3.3) satisfies the important property of $\mathcal{P}_3$ *Shape-preserving*. $q_j(x)$ has the same shape as $\sum_{i=j-1}^{j+1}\bar{w}^n_i\chi_i$, that is,

- $q_j(x)$ is monotone (on I_j) iff the cell averages $\{\bar{w}^n_{j-1}, \bar{w}^n_j, \bar{w}^n_{j+1}\}$ are;
- $q_j(x)$ admits an extremum value in the interior of I_j iff $\bar{w}^n_j$ is an extremum value (w.r.t $\bar{w}^n_{j\pm1}$).

The shape preserving property $\mathcal{P}_3$ tells us that the piecewise-parabolic reconstruction, $w(x, t^n) = \sum_j q_j(x)\chi_j(x)$, creates no new extrema at the *interior* of the cells, I_j's; thus, spurious extrema, if any, can be created *only* at interfaces where

$$sgn(q_{j+1}(x_{j+\frac{1}{2}}) - q_j(x_{j+\frac{1}{2}})) \neq sgn(\bar{w}^n_{j+1} - \bar{w}^n_j).$$

To avoid such spurious extrema, we now turn to the last (– and essential) step of *limiting* the reconstruction. To this end we consider convex modification of the form

$$(3.4) \qquad\qquad p_j(x) = \bar{w}^n_j + \theta_j(q_j(x) - \bar{w}^n_j), \quad 0 < \theta_j < 1.$$

Since $p'_j(x) = \theta_j q'_j(x)$, properties $\mathcal{P}_1$ and $\mathcal{P}_3$ remain valid. Moreover, a limiter θ_j is sought so that $(1 - \theta_j)$ is proportional to the interface jump, $q_{j+1}(x_{j+\frac{1}{2}}) - q_j(x_{j+\frac{1}{2}})$; by the third-order accuracy of $q(\cdot)$, the size of this jump — and hence of $(1 - \theta_j)$, is of order $\mathcal{O}((\Delta x)^3)$, and hence the modified quadratic, $p_j(x)$ remains third-order accurate (— property $\mathcal{P}_2$). Finally, it remains to specify θ_j so as to eliminate spurious interface extrema. One constructs such a limiter θ_j in terms of the cell quantities,

$$(3.5) \qquad\qquad M_j = \max_{x \in I_j} q_j(x), \quad m_j = \min_{x \in I_j} q_j(x),$$

(one need not actually compute these extremal values as we shall clarify in a moment), and,

$$(3.6) \qquad \begin{cases} M_{j\pm\frac{1}{2}} & = & \max\left\{\frac{1}{2}(\bar{w}^n_j + \bar{w}^n_{j\pm1}), q_{j\pm1}(x_{j\pm\frac{1}{2}})\right\}, \\ m_{j\pm\frac{1}{2}} & = & \min\left\{\frac{1}{2}(\bar{w}^n_j + \bar{w}^n_{j\pm1}), q_{j\pm1}(x_{j\pm\frac{1}{2}})\right\}. \end{cases}$$

The limiter θ_j is then given by

$$(3.7) \quad \theta_j \quad = \quad \begin{cases} \min\left\{\dfrac{M_{j+\frac{1}{2}} - \bar{w}^n_j}{M_j - \bar{w}^n_j}, \dfrac{m_{j-\frac{1}{2}} - \bar{w}^n_j}{m_j - \bar{w}^n_j}, 1\right\}, & \text{if} \quad \bar{w}^n_{j-1} < \bar{w}^n_j < \bar{w}^n_{j+1}, \\[4mm] \min\left\{\dfrac{M_{j-\frac{1}{2}} - \bar{w}^n_j}{M_j - \bar{w}^n_j}, \dfrac{m_{j+\frac{1}{2}} - \bar{w}^n_j}{m_j - \bar{w}^n_j}, 1\right\}, & \text{if} \quad \bar{w}^n_{j-1} > \bar{w}^n_j > \bar{w}^n_{j+1}, \\[4mm] 1 & \text{otherwise (if } \Delta_+\bar{w}^n_j \cdot \Delta_-\bar{w}^n_j < 0). \end{cases}$$

---

[1] We denote, as usual, $\Delta_\pm w(x) = \pm(w(x \pm \Delta x) - w(x))$ and $\Delta_0 = \frac{1}{2}(\Delta_+ + \Delta_-)$

Remark. We observe that the limiter θ_j is 'switched-on' only when the cell averages, $\{\bar{w}_{j-1}^n, \bar{w}_j^n, \bar{w}_{j+1}^n\}$, form a monotone sequence, which in turn, by the shape-preserving property $\mathcal{P}_3$, implies that $q_j(x)_{|x \in I_j}$ is monotone. Hence, the pair of cell quantities $\{M_j, m_j\}$ in (3.5) is simply given either by $\{q_j(x_{j+\frac{1}{2}}), q_j(x_{j-\frac{1}{2}})\}$ in the first (increasing) case, or by $\{q_j(x_{j-\frac{1}{2}}), q_j(x_{j+\frac{1}{2}})\}$ in the second (decreasing) case.

It was shown in [LO] that with this choice of θ_j's, the resulting quadratic reconstruction satisfies

$\mathcal{P}_4$ *Non-oscillatory property.* The piecewise-quadratic reconstruction is non-oscillatory in the sense that

$$(3.8) \qquad sgn(p_{j+1}(x_{j+\frac{1}{2}}) - p_j(x_{j+\frac{1}{2}})) = sgn(\bar{w}_{j+1}^n - \bar{w}_j^n).$$

In summary, the resulting piecewise parabolic reconstruction, $w(x, t^n) = \Sigma p_j(x) \chi_j(x)$, consists of quadratic pieces of the form

$$(3.9) \qquad p_j(x) = w_j^n + w_j' \left(\frac{x - x_j}{\Delta x}\right) + \frac{1}{2} w_j'' \left(\frac{x - x_j}{\Delta x}\right)^2.$$

Here, w_j'' are the (pointvalues of) the *reconstructed second derivatives*

$$(3.10) \qquad w_j'' := \theta_j \Delta_+ \Delta_- \bar{w}_j^n;$$

w_j' are the (pointvalues of) the *reconstructed slopes,*

$$(3.11) \qquad w_j' := \theta_j \Delta_0 \bar{w}_j^n;$$

and w_j^n are the *reconstructed pointvalues*

$$(3.12) \qquad w_j^n := \bar{w}_j^n - \frac{w_j''}{24}.$$

Observe that, starting with third- (and higher-) order accurate methods, pointwise values *cannot* be interchanged with cell averages, $w_j^n \neq \bar{w}_j^n$.

By properties $\mathcal{P}_1$ and $\mathcal{P}_2$, $w(x_1, t^n) = \Sigma p_j(x) \chi_j(x)$ is a third-order cell conservative reconstruction. By properties $\mathcal{P}_3$ and $\mathcal{P}_4$, it is a *non-oscillatory* reconstruction in the sense that $N(w(\cdot, t^n))$ — the number of extrema of $w(x, t^n)$, does not exceed that of its piecewise-constant projection, $N(\Sigma \bar{w}_j^n \chi_j(\cdot))$,

$$(3.13) \qquad N(w(\cdot, t^n)) \leq N(\Sigma \bar{w}_j^n \chi_j(\cdot)).$$

We close this section by noting that one can further modify the limiter θ_j in (3.5)-(3.7), consult [LO], so that the resulting quadratic reconstruction (3.9)-(3.12) satisfies — in addition to the NED property (3.13), also the *strict maximum principle* property, $\|w(\cdot, t^n)\|_{L^\infty} \leq \|\Sigma \bar{w}_j^n \chi_j(\cdot)\|_{L^\infty}$. Consequently, the corresponding third-order reconstruction is total-variation non-increasing.

3.2. The third-order scheme – scalar equations. The third-order accurate reconstruction of §3.1 is evolved in time using the central Godunov-type framework outlined in (2.9),

$$(3.14) \qquad \bar{w}^{n+1}_{\nu+\frac{1}{2}} = \bar{w}^n_{\nu+\frac{1}{2}} - \frac{1}{\Delta x}\left[\int_{\tau=t^n}^{t^{n+1}} f(w(x_{\nu+1},\tau))d\tau - \int_{\tau=t^n}^{t^{n+1}} f(w(x_\nu,\tau))d\tau \right].$$

To this end we need to evaluate the staggered averages, $\{\bar{w}^n_{\nu+\frac{1}{2}}\}$, and to approximate the interface fluxes, $\left\{ \int_{\tau=t^n}^{t^{n+1}} f(w(x_j,\tau))d\tau \right\}$.

With $p_j(x) = w^n_j + w'_j\left(\frac{x-x_j}{\Delta x}\right) + \frac{1}{2}w''_j\left(\frac{x-x_j}{\Delta x}\right)^2$ specified in (3.9)-(3.12), one evaluates the staggered averages of the third order reconstruction $w(x,t^n) = \Sigma p_j(x)\,\chi_j(x)$

$$(3.15) \qquad \bar{w}^n_{\nu+\frac{1}{2}} = \frac{1}{\Delta x}\int_{x_\nu}^{x_{\nu+1}} w(x,t^n)dx = \frac{1}{2}(\bar{w}_\nu + \bar{w}_{\nu+1}) + \frac{1}{8}(w'_\nu - w'_{\nu+1}).$$

Remarkably, we obtain here the same formula for the staggered averages as in the second-order cases, consult (2.15); the only difference is the use of the new limited slopes in (3.11), $w'_j = \theta_j\Delta_0\bar{w}^n_j$.

Next, we approximate the (exact) numerical fluxes by Simpson's quadrature rule, which is (more than) sufficient for retaining the overall third-order accuracy,

$$(3.16) \qquad \frac{1}{\Delta x}\int_{\tau=t^n}^{t^{n+1}} f(w(x_\nu,\tau))d\tau \sim \frac{\lambda}{6}\left[f(w^n_\nu) + 4f(w^{n+\frac{1}{2}}_\nu) + f(w^{n+1}_\nu) \right].$$

This in turn, requires the three approximate *pointvalues* on the right, $w^{n+\beta}_\nu \sim w(x_\nu,t^{n+\beta})$ for $\beta = 0,\frac{1}{2},1$. Following our approach in the second-order case, [NT], we use Taylor expansion to *predict*

$$(3.17) \qquad w^n_\nu \equiv w(x_\nu,t^n) = \bar{w}^n_\nu - \frac{w''_\nu}{24},$$

$$(3.18) \qquad w^{n+\frac{1}{2}}_\nu = w^n_\nu + \frac{\lambda}{2}\dot{w}^n_\nu + \frac{\lambda^2}{8}\ddot{w}^n_\nu,$$

$$(3.19) \qquad w^{n+1}_\nu = w^n_\nu + \lambda\dot{w}^n_\nu + \frac{\lambda^2}{2}\ddot{w}^n_\nu.$$

Here, the first couple of time derivatives on the right are evaluated by exact differentiation of the quadratic reconstruction (3.9) (here and below, $a(u)$ denotes the local speed, $a(u) := f_u(u)$),

$$(3.20) \qquad w^n_\nu = \bar{w}^n_\nu - \frac{w''_\nu}{24};$$

$$(3.21) \qquad \dot{w}^n_\nu \equiv (\Delta x \cdot \partial_t)w(x_\nu,t^n) = -\Delta x \cdot \partial_x f(w(x_\nu,t^n)) = -a(w^n_\nu)\cdot w'_\nu,;$$

$$(3.22) \qquad \ddot{w}^n_\nu \equiv (\Delta x \cdot \partial_t)^2 w(x_\nu,t^n) = \Delta x \cdot \partial_x\left[a(w^n_\nu)\Delta x \cdot \partial_x f(w(x_\nu,t^n))\right] =$$
$$= a^2(w^n_\nu)w''_\nu + 2a(w^n_\nu)a'(w^n_\nu)(w'_\nu)^2.$$

These evaluations of Taylor expansions could be substituted by the more economical Runge-Kutta integrations; the simplicity becomes more pronounced with *systems* which is the next issue in our discussion.

In summary of the scalar setup, we end up with a two step scheme where, starting with the reconstructed pointvalues

$$(3.23) \qquad w_\nu^n = \bar{w}_\nu^n - \frac{w_\nu''}{24},$$

we *predict* the pointvalues $w_\nu^{n+\beta}$ by, e.g. Taylor expansions,

$$(3.24) \qquad w_\nu^{n+\beta} = w_\nu^n + \lambda\beta \dot{w}_\nu^n + \frac{(\lambda\beta)^2}{2}\ddot{w}_\nu^n, \qquad \beta = \frac{1}{2}, 1;$$

this is followed by the *corrector* step

$$(3.25) \quad \bar{w}_{\nu+\frac{1}{2}}^n = \frac{1}{2}\left(\bar{w}_\nu^n + \bar{w}_{\nu+1}^n\right) \; + \; \frac{1}{8}\left(w_\nu' - w_{\nu+1}'\right) +$$
$$- \frac{\lambda}{6}\left\{\left[f(w_{\nu+1}^n) + 4f(w_{\nu+1}^{n+\frac{1}{2}}) + f(w_{\nu+1}^{n+1})\right]\right.$$
$$\left. - \left[f(w_\nu^n) + 4f(w_\nu^{n+\frac{1}{2}}) + f(w_\nu^{n+1})\right]\right\}.$$

3.3. The third-order scheme – systems.

We use the ingredients of the scalar scheme in §3.2, to construct the third-order approximation for systems of conservation laws. The attractive feature is simplicity – these Riemann-free ingredients involve simple algebraic manipulations which admits a straightforward *component-wise* extension to systems. By assembling the ingredients in §3.2 we arrive at the following predictor-corrector scheme.

First, we *predict the pointvalues*, $w_\nu^{n+\beta}$, $\beta = \frac{1}{2}, 1$,

$$(3.26) \qquad w_\nu^{n+\beta} = w_j^n - \lambda\beta A_\nu^n w_\nu' + \frac{(\lambda\beta)^2}{2}\left\{(A_\nu^n)^2 w_\nu'' + 2A_\nu^n B_\nu^n[w_\nu', w_\nu']\right\}.$$

Here, $A_\nu^n \equiv A(w_\nu^n)$ and $B_\nu^n = B(w_\nu^n)$ are, respectively, the Jacobian of $f(\cdot)$, $A_{ij} = \frac{\partial f_i}{\partial u_j}$, and the corresponding 3-tensor, $B_{ijk} = \frac{\partial f_i}{\partial u_j \partial u_k}$, and w_ν^n, w_ν', w_ν'' are the vectors of pointvalues and their couple of derivatives, derived from the non-oscillatory quadratic reconstruction in §3.1:

$$\begin{aligned} w_\nu'' &= \Theta_\nu\left(\bar{w}_{\nu+1}^n - 2\bar{w}_\nu^n + \bar{w}_{\nu-1}^n\right) \\ w_\nu' &= \frac{1}{2}\Theta_\nu\left(\bar{w}_{\nu+1}^n - \bar{w}_{\nu-1}^n\right) \\ w_\nu &= \bar{w}_\nu^n - \frac{1}{24}w_\nu''. \end{aligned}$$

A couple of remarks is in order.
- *The limiter.* Here we include the possibility of a *matrix* limiter, Θ_ν, which takes into account Roe-like decompositions into characteristic waves [Ro]. As already noted in [NT], however, one of the main advantages of our central-staggered framework over that of the upwind schemes, is that such expensive

and time-consuming characteristic decompositions can be avoided. Specifically, all the non-oscillatory computations reported in §5 below were carried out with diagonal limiters, Θ_ν, based on a *component-wise* extension of the scalar limiters outlined in (3.5)-(3.7).

- *Taylor vs. Runge-Kutta expansion.* There is a variety of more economical alternatives to Taylor expansion used for the predictor step in (3.26). For example, the explicit evaluation of the 3-tensor B_ν^n on the right of (3.26) can be avoided if the exact spatial derivatives inside the curly brackets on the right of (3.26), $(A^2 w_x)_x$, are replaced by an approximate discrete one, $\{\cdot\}_\nu' := \Theta_\nu \Delta_0 \{\cdot\}_\nu$,

$$(3.26') \qquad w_\nu^{n+\beta} = w_\nu^n - \lambda\beta A_\nu^n w_\nu' + \frac{(\lambda\beta)^2}{2} \{(A_\nu^n)^2 w_\nu'\}'.$$

Still another alternative which utilizes the discrete derivative, is the second-order Runge-Kutta, which reads

$$(3.26'') \qquad w_\nu^{n+\beta} = w_\nu^n - \lambda\beta \left\{ f\left(w_\nu^n - \frac{\lambda\beta}{2} A_\nu^n w_\nu' \right) \right\}'.$$

And an even more greedy version is the second-order Runge-Kutta which does not require the computation of any Jacobian,

$$(3.26''') \qquad w_\nu^{n+\beta} = w_\nu^n - \lambda\beta \left\{ f\left(w_\nu^n - \frac{\lambda\beta}{2} \left\{ f(w_\nu^n) \right\}' \right) \right\}'.$$

The numerical experiments reported in this paper utilize the predictor step in its basic version (3.26). As expected, its exactly differentiated terms seem to provide a slightly more accurate results than the more economical versions in (3.26')-(3.26'''). We should point out, however, that the latter, Jacobian-free versions (3.26'-3.26'''), are still offering economical alternatives – our numerical experiments, e.g., [TW], show that they retain essentially the same high-resolution as the basic version (3.26).

Equipped with the predicted pointvalues in (3.26), together with Simpson's quadrature (3.16), we evaluate the approximate flux, $f_\nu^{n+\frac{1}{2}}$,

$$(3.27') \qquad f_\nu^{n+\frac{1}{2}} := \frac{1}{6} \left[(f(w_\nu^n) + f(w_\nu^{n+\frac{1}{2}}) + f(w_\nu^{n+1}) \right];$$

these approximate fluxed are then used with the exact staggered averaging, (3.15), in order to evaluate the cell averages of the next time level, $t = t^{n+1}$, by the central recipe (3.14),

$$(3.27'') \qquad \bar{w}_{\nu+\frac{1}{2}}^{n+1} = \frac{1}{2}(\bar{w}_\nu^n + \bar{w}_{\nu+1}^n) + \frac{1}{8}(w_\nu' - w_{\nu+1}') - \lambda\left[f_{\nu+1}^{n+\frac{1}{2}} - f_\nu^{n+\frac{1}{2}} \right],$$

The predictor-corrector scheme (3.26)–(3.27''), expressed in terms of the pointwise limited derivatives, w_ν^n, w_ν' and w_ν'', form our third-order non-oscillatory central scheme.

4. Stability of the scalar scheme (the NED property). In this section we make a precise assertion regarding the non-oscillatory behavior of our third-order central scheme in the scalar case.

Our starting point is the *exact* staggered averaging of the scalar piecewise-quadratic reconstruction, $w(x, t^n) = \sum_j [w_j^n + w_j' \left(\frac{x-x_j}{\Delta x}\right) + \frac{1}{2} w_j'' \left(\frac{x-x_j}{\Delta x}\right)^2] \chi_j$, which yields the corrector scheme (3.14)-(3.15)

$$
(4.1) \quad \bar{w}_{\nu+\frac{1}{2}}^{n+1} = \frac{1}{2}(\bar{w}_\nu + \bar{w}_{\nu+1}) +
$$
$$
+ \frac{1}{8}(w_\nu' - w_{\nu+1}') - \frac{1}{\Delta x}\left[\int_{\tau=t^n}^{t^{n+1}} f(w_{\nu+1}(\tau))d\tau - \int_{\tau=t^n}^{t^{n+1}} f(w_\nu(\tau))d\tau\right].
$$

Here, $w_\nu(\tau) = w(x_\nu, \tau \geq t^n)$ are the mid-cells pointvalues governed by, consult (2.13)

$$
(4.2) \qquad w_t + f(w)_x = 0, \quad \tau \geq t^n,
$$

$$
(4.3) \qquad w(x, \tau = t^n) = w_\nu^n + w_\nu'\left(\frac{x-x_\nu}{\Delta x}\right) + \frac{1}{2}w_\nu''\left(\frac{x-x_\nu}{\Delta x}\right)^2, \quad x \in I_\nu.
$$

To *approximate* the temporal integrals on the right of (4.1), Simpson's quadrature rule, (3.16), followed by Taylor expansions, (3.17)-(3.19), were used. We note that, at least in the scalar case under consideration, one can evaluate these integrals *exactly* in a straightforward manner. Indeed, thanks to the central staggering, the mid-cells $(x_\nu, \tau \geq t^n)$ are 'secured' inside a smooth region where the local speed $a(w_\nu(\tau))$ satisfies a simple quadrature whose solution yields

$$
a(w_\nu(\tau)) = \frac{w_\nu^n}{1 + sw_\nu'}\left[1 + \frac{w_\nu \cdot s^2 w_\nu''}{2(1 + sw_\nu')^2} + \mathcal{O}(s^4)\right], \qquad s := \frac{\tau - t^n}{\Delta x}.
$$

Our first main result asserts the non-oscillatory behavior of the central scheme (4.1) based on the above mentioned *exact* flux evaluation.

PROPOSITION 4.1. *Consider the central scheme (4.1)-(4.3), based on the third-order accurate quadratic reconstruction, (3.9)-(3.12). Then it satisfies the so-called Number of Extrema Diminishing (NED) property, in the sense that*

$$
(4.4) \qquad N\left(\sum_\nu \bar{w}_{\nu+\frac{1}{2}}^{n+1} \chi_{\nu+\frac{1}{2}}(x)\right) \leq N\left(\sum_\nu \bar{w}_\nu^n \chi_\nu(x)\right).
$$

Proof. We first recall that the quadratic reconstruction, $w(\cdot, t^n)$, in (3.9)-(3.12) is non-oscillatory in the sense of satisfying the NED property, consult (3.13),

$$
N(w(\cdot, t^n)) \leq N\left(\sum_\nu \bar{w}_\nu^n \chi_\nu(\cdot)\right).
$$

Next we consider the *sliding average* of the reconstruction, $\bar{w}(x, t^n) = \frac{1}{\Delta x}\int_{I_x} w(\xi, t^n)d\xi$; clearly, since $\bar{w}(\cdot, t) = w(\cdot, t^n) * \frac{1}{\Delta x}\chi_0$, with the positive mollifier $\frac{1}{\Delta x}\chi_0$, we have

$$
N(\bar{w}(\cdot, t^n)) \leq N(w(\cdot, t^n)).
$$

Finally, we study the governing equation for $\bar{w}(\cdot, t)$: by averaging (4.3) we find an averages-pointvalues relation similar to (2.2), which we rewrite as

$$(4.5) \qquad \bar{w}_t(x, t) + \tilde{a}(x, t)\bar{w}_x(x, t) = 0.$$

Here, $\tilde{a}$ denotes the averaged speed, $\tilde{a} := \int_{\eta=0}^{1} a[w(x - \frac{\Delta x}{2}, t) + \eta \Delta w(x - \frac{\Delta x}{2}, t)]d\eta$. Thus, the sliding average, $\bar{w}(\cdot, t)$, is a C^1-solution of the *transport equation* (4.5), and as such it satisfies

$$N(\bar{w}(\cdot, t^{n+1})) \leq N(\bar{w}(\cdot, t^n)).$$

In particular, by sampling at the mid-cells $(x_{\nu+\frac{1}{2}}, t^{n+1})$, we have $N\left(\sum_\nu \bar{w}_{\nu+\frac{1}{2}}^{n+1} \chi_{\nu+\frac{1}{2}}(x)\right) \leq N(\bar{w}(\cdot, t^{n+1}))$. This, together with the previous last three inequalities yields the NED property (4.4). $\blacksquare$

Remarks.

1. Harten and Osher proved the NED property for their *uniformly* second-order non-oscillatory scheme [HO]. In particular, the NED property enables to circumvent the limitation of first-order clipping phenomena in TVD schemes [OT]. (Observe that the limiter θ_j in (3.7) is *not* 'switched-on' at extrema where $\theta_j = 1$. If instead, we set $\theta_j = 0$ in those cases, we run into the familiar 'clipping' phenomena, where we avoid increasing extrema, at the expense of reducing to the first-order accurate LxF scheme).

2. Let $TV(\bar{w}(\cdot, t^n)) = \sum_\nu |\bar{w}_{\nu+1}^n - \bar{w}_\nu^n|$ denote the total-variation of the piecewise-constant approximation of $t = t^n$, then the following straightforward upper-trend holds

$$TV(\bar{w}(\cdot, t^n)) \leq 2N\left(\sum_\nu \bar{w}_\nu^n \chi_\nu(\cdot)\right) \|\sum \bar{w}_\nu^n \chi_\nu(\cdot)\|_{L^\infty}.$$

Thus, the NED property together with an additional L^∞-bound imply Total Variation boundedness $TV(\bar{w}(\cdot, t^n)) \leq$ Const., and hence the convergence of the approximate solutions.

3. As we have already noted before, one can modify the limiter in (3.5)-(3.7), consult [LO], so that the resulting quadratic reconstruction (3.9)-(3.12) satisfies a (strict) maximum principle, in addition to the NED property. Consequently, the corresponding third-order central scheme (4.1)-(4.3) based on such modified limiter, is total-variation bounded and hence convergent. We found, however, that the enforcement of an additional (strict) maximum principle is neither necessary (in the scalar case), nor is it recommended for systems (which need not satisfy a *component-wise* maximum principle). Finally, our numerical experiments also show that the conclusion of Proposition 4.1 remains valid with Simpson's rule (3.16) replacing the exact flux evaluations on the right of (4.1).

5. Numerical experiments.

5.1. Scalar conservation laws. In this section we use some model problems to numerically test our schemes, (3.23)–(3.25). In the scalar context, we used the modified nonoscillatory limiter, which enforces the (strict) maximum principle, [LO].

Example 1 (Transport equation). We solve the model transport equation

$$(5.1) \qquad\qquad u_t + u_x = 0, \qquad -1 \le x \le 1,$$

subject to 2-periodic initial data, $u(x, 0) = u_0(x)$.

Two sets of initial data $u_0(x)$ were used: the first one is $u_0(x) = sin(\pi x)$; Table 5.1 quotes the L^1 and L^∞ errors at $t = 10$. The second one is $u_0(x) = sin^4(\pi x)$, and we list the errors, recorded at time $t = 1$. in Table 5.2.

Remark. Here, and in all the examples below, N denotes the total number of spatial cells, and Δx is the gridsize given by $\Delta x = \frac{2}{N}$. L^p errors are measured by the difference between the pointvalues of the "exact" solution, $u(x_\nu, t^n)$, and the *reconstructed* pointvalues of the computed solution (consult (3.12)), $w_\nu^n = \bar{w}_\nu^n - \frac{1}{24} w_\nu''$.

For these two sets of initial data, we obtain third-order of accuracy in the smooth region in both L^1 and L^∞ norms. We note that standard ENO approximations of (5.1) with the second set of initial data, experiences an (easily fixed) loss of accuracy, see [RM], [Sh]. No such degeneracy was found with our present method. Indeed, as noted by Shu, [Sh], the class of centered schemes are particularly good candidates — in term of uniform convergence, independently of the initial data.

N	L^1 error	L^1 order	L^∞ error	L^∞ order
20	5.9860820848605D-03		4.6594637767945D-03	
40	7.2221473780366D-04	3.05	5.6598067445823D-04	3.04
80	8.8393644258658D-05	3.03	6.9389462422187D-05	3.03

Table 5.1: Linear transport equation (5.1) with $u_0 = \sin(\pi x)$. Errors at $t = 10$. (mesh-ratio $\lambda = 0.45$).

N	L^1 error	L^1 order	L^∞ error	L^∞ order
20	3.6847016242948D-02		4.7637603673449D-02	
40	4.2469435064558D-03	3.11	5.6195017130236D-03	3.08
80	5.7429143455091D-04	2.89	6.1346629453563D-04	3.20

Table 5.2: Linear transport equation (5.1) with $u_0 = \sin^4(\pi x)$. Errors at $t = 1$. (mesh-ratio $\lambda = 0.45$).

Example 2 (Propagation of singularities). Here we consider the transport equation (5.1) initialized with the 2-periodic *discontinuous* characteristic function, $u_0(x) = \chi_0 = 1_{-\frac{1}{2} \le x \le \frac{1}{2}}$. We observe the good resolution of the computed solution in Figure 5.1. As

expected, the viscous profile spreads over a transition layer of sizes $(\Delta x)^{\frac{3}{4}}$, sharpening the first- and second-order shock layers of the corresponding size $\sqrt{\Delta x}$ and $(\Delta x)^{\frac{2}{3}}$. This sharpening will be borne out in our later numerical experiments, with the improved resolution of contact discontinuities in the system of Euler's equations.
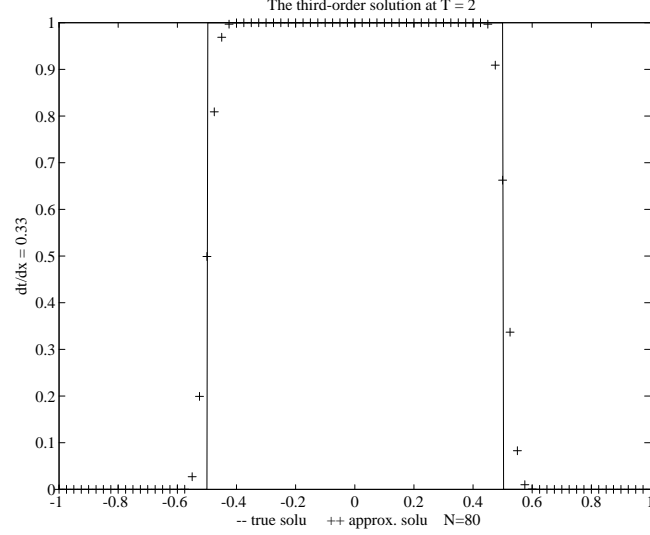

Fig. 5.1: Linear transport equation (5.1) with $u_0 = 1_{-\frac{1}{2} \leq x \leq \frac{1}{2}}$ computed at $t = 2$. (mesh-ratio $\lambda = 0.45$).

Example 3 (Nonlinear transport equation). We solve the canonical, inviscid Burgers' equation

$$(5.2) \qquad u_t + (\frac{1}{2}u^2)_x = 0, \qquad -1 \leq x \leq 1,$$

subject to 2-periodic initial data $u_0(x) = 1 + \frac{1}{2}sin(\pi x)$.

Recall that the exact solution is smooth up to the critical time $t = \frac{2}{\pi}$. In Table 5.3 we list the errors at $t = 0.3$. Note that we have close to third-order accuracy in L^1, and more than second-order of accuracy in L^∞.

N	L^1 error	L^1 order	L^∞ error	L^∞ order
80	4.2801323416700D-05		1.1326254561539D-04	
160	5.8285516297496D-06	2.87	2.3542917027330D-05	2.27
320	9.0492108000412D-07	2.69	4.9181998684755D-06	2.26
640	1.5906270083160D-07	2.51	1.0364502238680D-06	2.45
1280	2.7007985022899D-08	2.55	2.1676749817345D-07	2.26

Table 5.3: Inviscid Burgers' equation (5.2) with $u_0(x) = 1 + \frac{1}{2}sin(\pi x)$. Errors at $t = 0.3$ (mesh-ratio $\lambda = 0.33$).

At $t = \frac{2}{\pi}$, the Burgers' equation develops a moving shock which then interacts with a rarefaction wave; at $t = 1.1$ the interaction between the shock and the rarefaction waves is over, and the solution becomes monotone between shocks. In Figures (5.2)-(5.3) we observe the excellent agreement between the exact and the non-oscillatory computed solution, in both stages of the developed discontinuity. In particular, Table 5.4 records the L^1 and L^∞ errors in the smooth portion of the solution, bounded away from the moving discontinuity. Third-order accuracy in both in L^1 and L^∞ is observed in the smooth portion — at distance 0.1 away from the shock. The errors are of smaller magnitude than the ones in the smooth case, showing the reduction in error propagation.

Finally, we note that in figure (5.3) we record the results based on the two versions of the nonoscillatory limiter (3.5)-(3.7): the figure on the left utilizes the *modified* version which enforces the additional the maximum principle, [LO], and it is compared with the figure on the right, where the basic version of the NED limiter is used without the enforcement of an extra maximum principle. It is evident that we retain the same quality results in both cases. This promotes us to concentrate, in the case of systems, on the nonoscillatory limiter in its basic version, (3.5)-(3.7), without the extra enforcement of the maximum principle.
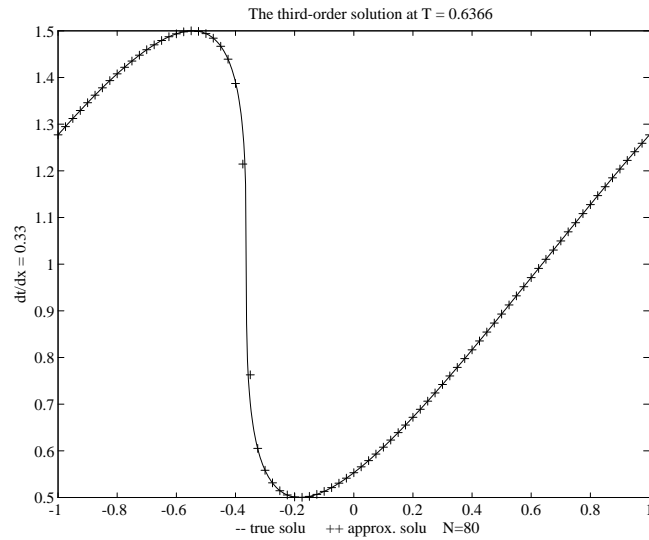

Fig. 5.2: Burgers' equation (5.2) with $u_0(x) = 1 + \frac{1}{2}sin(\pi x)$ computed at $t = 0.6366$.
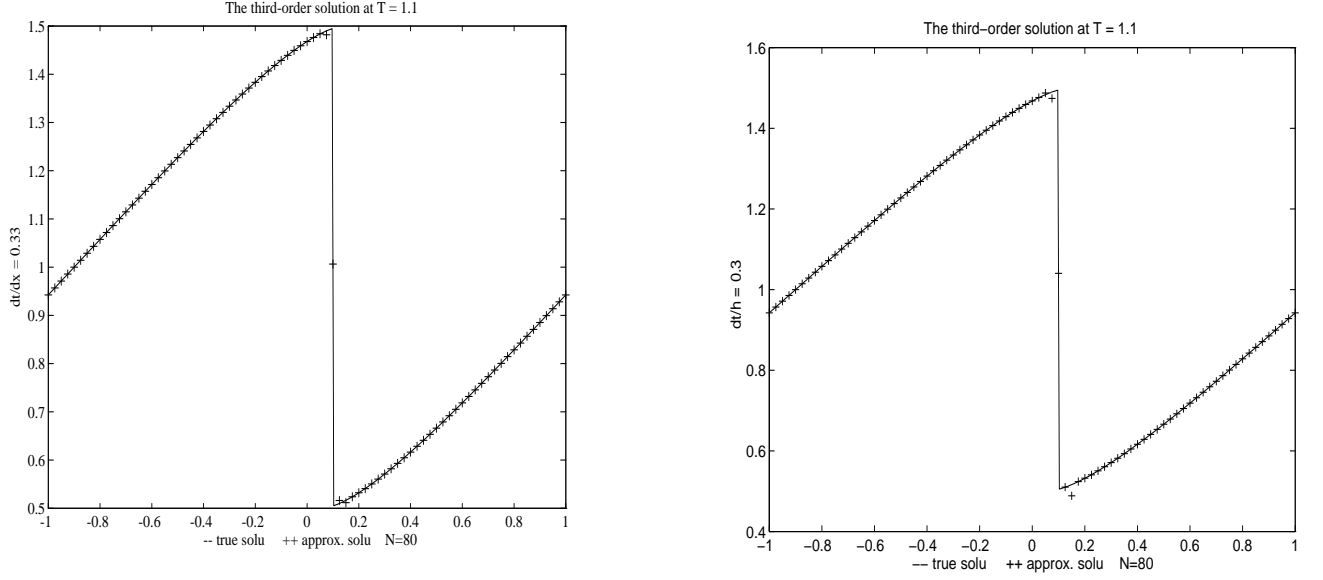
Fig. 5.3: Burgers' equation (5.2) with $u_0(x) = 1 + \frac{1}{2} sin(\pi x)$ computed at $t = 1.1$. Nonoscillatory limiter: with enforcement of maximum principle ($-$ on left) and without ($-$ on right).

N	L^1 error	L^1 order	L^∞ error	L^∞ order
160	1.0475469475579D-06		6.4049985024628D-06	
320	1.3581473560717D-07	2.95	7.9514987438856D-07	3.01
640	1.7194296121278D-08	2.98	1.0309250031426D-07	2.95

Table 5.4: Burgers' equation (5.2) with $u_0(x) = 1 + \frac{1}{2} sin(\pi x)$. L^1, L^∞ errors 0.1 away from the shock, i.e. $\mid x -$ shock location $\mid \geq 0.1$, at $t = 1.1$ (mesh-ratio $\lambda = 0.33$).

5.2. Euler equations of Gas Dynamics. In this subsection we apply our third-order scheme to the Euler equations of polytropic gas,

$$(5.3) \qquad\qquad u_t + f(u)_x = 0,$$

where $u = (\rho, m, E)^t$ is the unknown vector of density ρ, momentum, $m := \rho q$, and energy E, and $f(u)$ is the corresponding flux, $f(u) = qu + (0, p, qp)^t$ expressed in terms of the pressure, $p := (\gamma - 1)(E - \frac{1}{2}\rho q^2)$ with a fixed $\gamma = 1.4$.

Example 4 (Riemann problems). We consider the Riemann problems subject to Riemann initial data,

$$u_0(x) = \begin{cases} u_l & x < 0 \\ u_r & x > 0. \end{cases}$$

Two sets of Riemann initial data are used: the one proposed by Sod in [So],

(5.4) $$(\rho_l, m_l, E_l) = (1, 0, 2.5), \quad (\rho_r, m_r, E_r) = (0.125, 0, 0.25);$$

and the one used by Lax [La]:

(5.5) $$(\rho_l, m_l, E_l) = (0.445, 0.311, 8.928), \quad (\rho_r, m_r, E_r) = (0.5, 0, 1.4275).$$

Figure 5.4 shows the third-order central results for Sod's problem, in comparison to the corresponding second-order central results. Two major impovements should be pointed out:
{i} A narrow transion layer with a considerably sharper resolution of the contact wave (– an improvement already anticipated in the linear Example 2 above);
{ii} Third-order resolution improvement of the second-order results (– which is most evident at the rarefaction tips).

Figure 5.5 comapres the results of the third-order central scheme with the second-order upwind ULT scheme of Harten [Ha]. In this context (of different order of accuracy), we would like to emphasize the following two points:
{i} The sharper contact resolution by the third-order scheme;
{ii} The improved resolution, particularly near the rarefaction tips; very mild oscillations, however, are detected in the third-order computation of the velocity field. These are at the acceptable the level, once we take into account the simplicity and efficiency offered by our *componentwise* computation vs. the complexity of the upwind characteristic approach.

Example 5 (Double blast waves). Our last example taken from Woodward and Colella, [WC], describes the interaction of blast waves subject to initial conditions

(5.6) $$u_0(x) = \begin{cases} u_l & 0 \le x < 0.1, \\ u_m & 0.1 \le x < 0.9, \\ u_r & 0.9 \le x < 1, \end{cases}$$

with

(5.7) $$\begin{cases} (\rho_l, m_l, E_l) &= (1, 0, 1000), \\ (\rho_m, m_m, E_m) &= (1, 0, 0.01), \\ (\rho_r, m_r, E_r) &= (1, 0, 100). \end{cases}$$

A solid wall boundary conditions (reflection) is applied to both ends. In Figure 5.6 we compare the third-order numerical results at $t = 0.01$, with the corresponding second-order computations of [NT]. Here we would like to highlight:
{i} Sharper resolution of the shock waves;
{ii} Elimination of the extrema clipping which was evident in the second-order computation of the density in figure 5.6: observe that the density spike (on the right) has now the correct amplitude of ~ 5.2, up from the second-order 'clipped' value of ~ 3.7.
The numerical results computed at the later time, $t = 0.03$ and $t = 0.038$, are presented in Figure 5.7. It is remarkable that the third-order central scheme is able to obtain such sharp resolution of the complex double blast problem, *without* any use of characteristic information, additional artificial compression, add-hoc switches,etc.
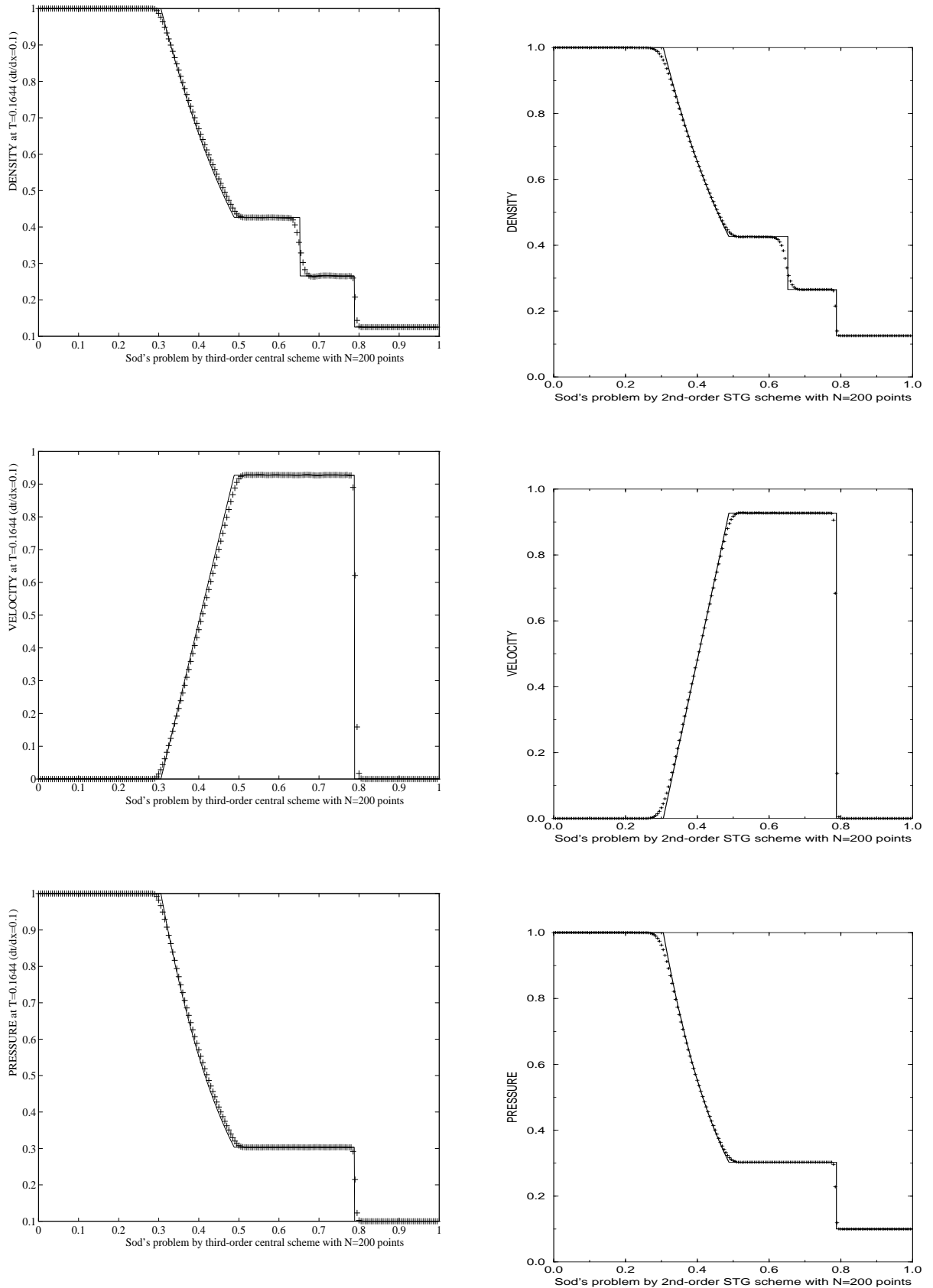
Fig. 5.4: Third- vs. second-order central schemes — Riemann problem with Sod's initial data (5.4) computed at $t = 0.1644$.
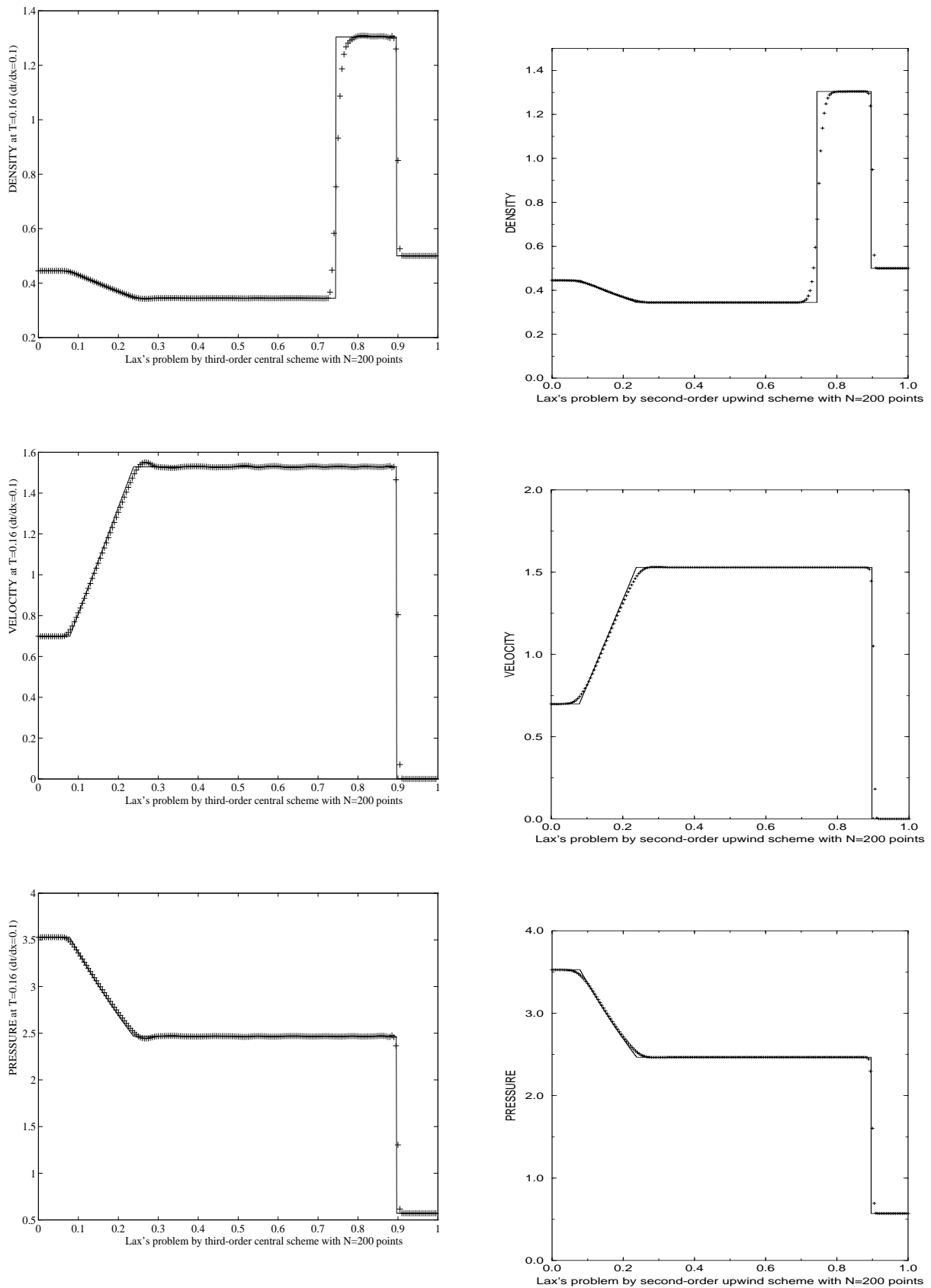
Fig. 5.5: Third-order central vs. second-order upwind schemes — Riemann problem with Lax's initial data (5.5) computed at $t = 0.16$.
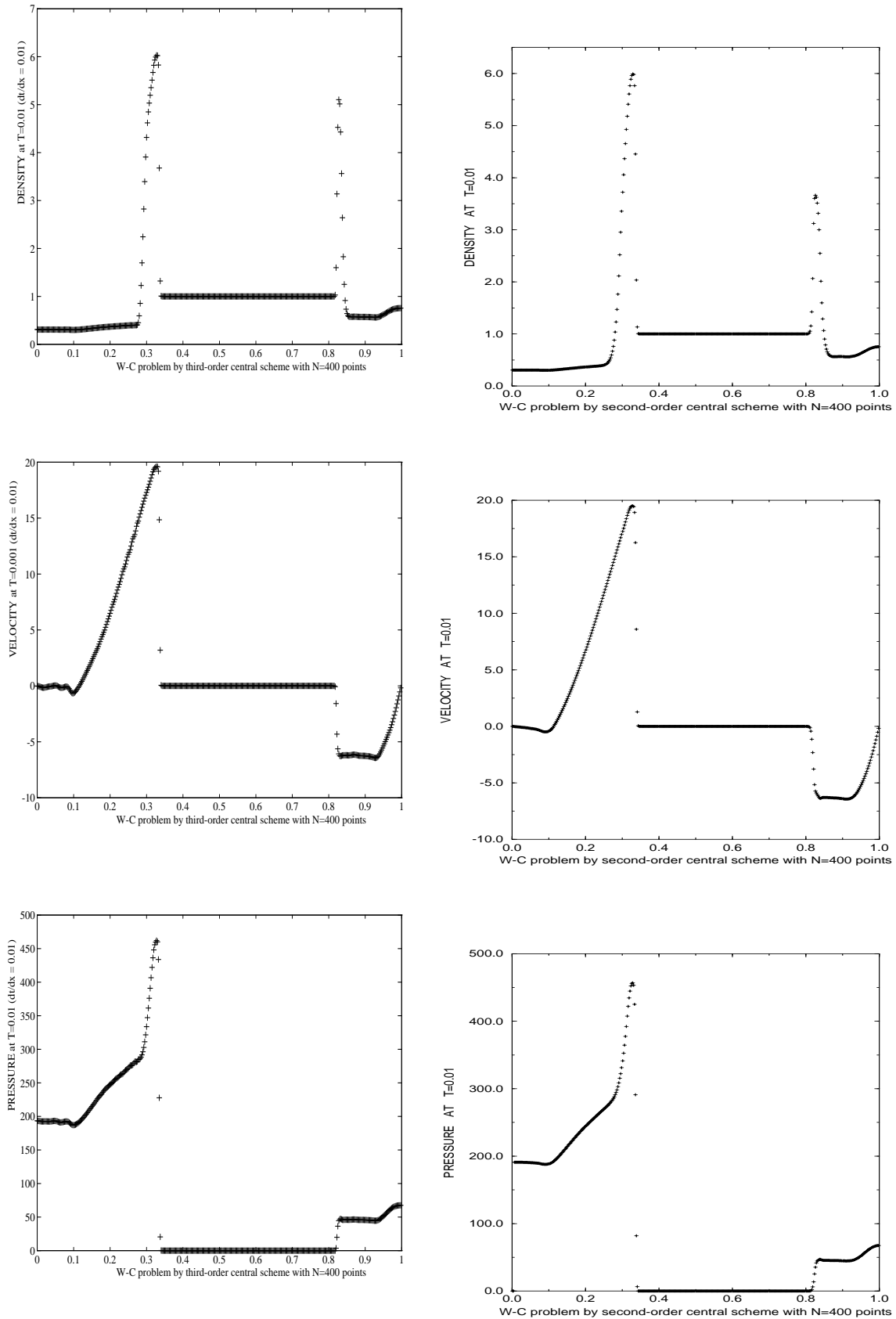
Fig. 5.6: Third- vs. second-order central schemes — Woodward-Colella double blast waves with initial data (5.7), computed at $t = 0.01$.
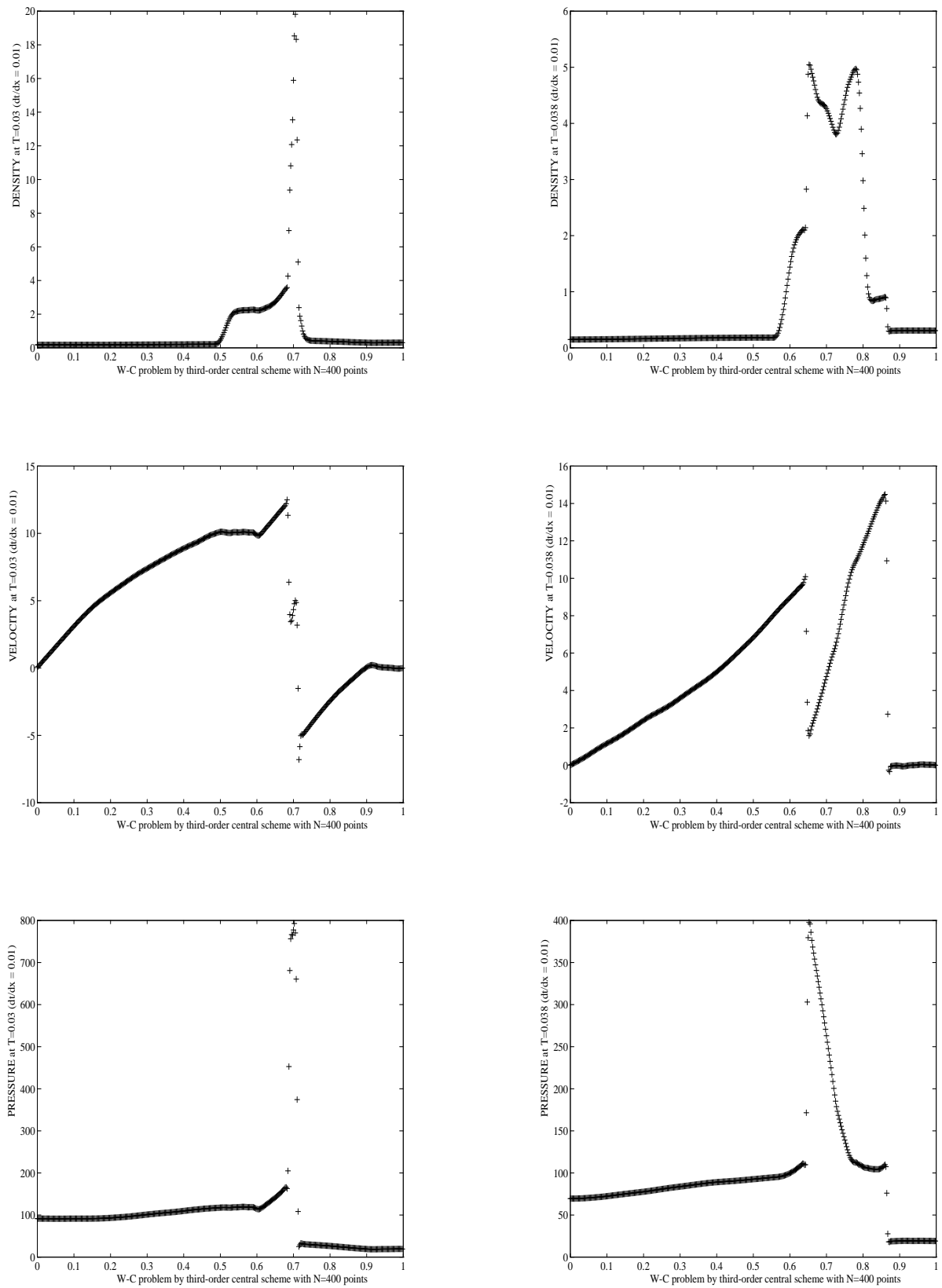
Fig. 5.7: Third-order central scheme — Woodward-Colella double blast waves with initial data (5.7), computed at $t = 0.03$ and $t = 0.038$.

REFERENCES

[ASV]   P. Arminjon, D. Stanescu and M.-C. Viallon, *A two-dimensional finite volume extension of the Lax-Friedrichs and Nessyahu-Tadmor schemes for compressible flows*, Proc. 6th Intl. Symp. on Comp. Fluid Dynamics (M. Hafez, K. Oshima eds.), Lake Tahoe, 1995.

[AV]   P. Arminjon and M.C. Viallon, *Généralisation du schéma de Nessyahu-Tadmor pour une équation. hyperbolique à deux dimensions d'espace*, C.R. Acad. Sci. Paris, t. 320, série I. 1995, pp. 85-88.

[BS]   F. Bereux and L. Sainsaulieu, *A Roe-type Riemann solver for hyperbolic systems with relaxation based on time-dependent wave decomposition*, Numer. Math. 77 (1997), pp. 143-185.

[CW]   P. Colella and P. Woodward, *The piecewise parabolic method (PPM) for gas-dynamical simulations*, JCP **54**, 1984, pp. 174-201.

[Er]   G. Erbes, *A high-resolution Lax-Friedrichs scheme for Hyperbolic conservation laws with source term. Application to the Shallow Water equations.* Preprint.

[Go]   S.K. Godunov, *A finite difference method for the numerical computation of discontinuous solutions of the equations of fluid dynamics*, Mat. Sb. **47**, 1959, pp. 271-290.

[Ha]   A. Harten, *High resolution schemes for hyperbolic conservation laws*, JCP **49**, 1983, pp. 357-393.

[HEOC] A. Harten, B. Engquist, S. Osher and S.R. Chakravarthy, *Uniformly high order accurate essentially non-oscillatory schemes. III*, JCP **71**, 1982, pp. 231-303.

[HO]   A. Harten and S. Osher, *Uniformly high order accurate non-oscillatory scheme. I*, SINUM **24**, 1982, pp. 229-309.

[Hu]   Huynh, *A piecewise-parabolic dual-mesh method for the Euler equations*, AIAA-95-1739-CP, The 12th AIAA CFD Conf., 1995.

[JT]   G. S. Jiang and E. Tadmor, *Non-oscillatory central schemes for multidimensional hyperbolic conservation laws*, SIAM J. Sci. Comput., in press.

[JX]   S. Jin and Z. Xin, *The relaxation schemes for systems of conservation laws in arbitrary space dimensions*, CPAM **48**, 1995, pp. 235-276.

[La]   P.D. Lax, *Weak solutions of non-nonlinear hyperbolic equations and their numerical computations*, CPAM **7**, 1954, pp. 159-193.

[Le]   B. van Leer, *Towards the ultimate conservative difference scheme, V. A second order sequel to Godunov's method*, JCP **32**, 1979, pp. 101-136.

[LL]   X.-D. Liu and P. D. Lax *Positive Schemes for Solving Multi-dimensional Hyperbolic Systems of Conservation Laws*, CFD Journal **5**, (1996), pp.1-24.

[LO]   X.-D. Liu and S. Osher, *Nonoscillatory high order accurate self similar maximum principle satisfying shock capturing schemes. I*, SINUM **33**, 1996, pp. 760-779..

[Ne]   N. Nessyahu, *Non-oscillatory second order central type schemes for systems of nonlinear hyperbolic conservation laws*, M.Sc. Thesis, Tel-Aviv University, 1987.

[NT]   N. Nessyahu and E. Tadmor, *Non-oscillatory central differencing for hyperbolic conservation laws*, JCP **87**, 1990, pp. 408-448.

[NTT]   H. Nessyahu, E. Tadmor and T. Tassa, *On the convergence rate of Godunov-type schemes*, SINUM **31**, 1994, pp. 1-16.

[OT]   S. Osher and E. Tadmor, *On the convergence of difference approximating to scalar conservation laws*, Math. Comp., **50**, 1988, pp. 15-51.

[Ro]   P. Roe, *Approximate Riemann solvers, parameter vectors, and difference schemes*, JCP **43**, 1981, pp. 357-372.

[RM]   A. Rogerson and E. Meiburg, *A numerical study of the convergence properties of ENO schemes*, J. Sci. Comput., **5**, 1990, pp. 127-149.

[Sa1]   R. Sanders, *A third-order accurate variation nonexpansive difference scheme for single conservation laws*, Math. Comp. **51**, 1988, 535-558.

[Sa2]   R. Sanders, Private communication.

[SW]   R. Sanders and A. Weiser, *A high resolution staggered mesh approach for nonlinear hyperbolic systems of conservation laws*, JCP **1010**, 1992, pp. 314-329.

[Sw]   P. Sweby, *High resolution schemes using flux limiters for Hyperbolic conservation laws*, SINUM

21, 1984, pp. 995-1001.

[Sh]   C.-W. Shu, *Numerical experiments on the accuracy of ENO and modified ENO schemes*, JCP **5**, 1990, pp. 127-149.

[So]   G. Sod, *A survey of several finite difference methods for systems of nonlinear hyperbolic conservation laws*, JCP **22**, 1978, pp. 1-31.

[TW]   E. Tadmor and C.C. Wu, *Central scheme for the multidimensional MHD equations*, in preparation.

[WC]   P. Woodward and P. Colella, *The numerical simulation of two-dimensional fluid flow with strong shocks*, JCP **54**, 1988, pp. 115-173.